IAC-18,C4,3,6,x47333

HYBRID ROCKETS WITH NOZZLE IN ULTRA-HIGH-TEMPERATURE CERAMIC COMPOSITES

Giuseppe D. Di Martino[a*], Stefano Mungiguerra[a], Anselmo Cecere[a], Raffaele Savino[a], Antonio Vinci [b], Luca Zoli[b], Diletta Sciti[b]

[a] *University of Naples "Federico II", Department of Industrial Engineering, P.le Vincenzo Tecchio 80, 80125 Napoli, Italy*
[b] *National Research Council, Institute of Science and Technology for Ceramics, Via Granarolo 64, 48018 Faenza, Italy*
* Corresponding Author, e-mail: giuseppedaniele.dimartino@unina.it

Abstract

In the framework of the Horizon 2020 project C^{3}HARME, an experimental campaign has been carried out to characterize a new class of Ultra-High-Temperature Ceramic Matrix Composites (UHTCMC) for near-zero erosion rocket nozzles. A novel test set-up has been developed to the purpose of testing small-sized specimens, with ZrB_2-based matrix and carbon fibers, exposing them to the supersonic exhaust plume of a 200N-class hybrid rocket nozzle, employing gaseous oxygen as oxidizer and High-Density PolyEthylene as fuel. The aim of the tests was to reproduce realistic rocket nozzles operating conditions, in order to demonstrate the ability of the specimens to preserve their functional integrity in a relevant environment. After that a UHTCMC nozzle throat insert has been manufactured and experimentally tested to verify the erosion resistance and evaluate the effects on the rocket performance by comparison with those obtained in similar operating conditions employing a graphite nozzle. Computational Fluid Dynamics simulations supported the experimental activities allowing for the rebuilding of the thermo-fluid-dynamic and chemical flow field and the characterization of the test conditions.

Keywords: Ultra-High-Temperature Ceramic Matrix Composites; Hybrid rocket nozzle; Near-zero erosion; Computational Fluid Dynamic simulation

Nomenclature

A_k	Arrhenius rate pre-exponential factor
A_t	Nozzle throat section area
a, n	Regression rate law constants
C*	Characteristic velocity
D	Fuel grain port diameter
E_a	Activation energy
G	Mass flux
K	Arrhenius rate
L	Fuel grain length
$\dot{m}$	Mass flow rate
OF	Oxidizer-to-fuel ratio
p_c	Chamber pressure
R	Universal gas constant
$\dot{r}$	Regression rate
T	Temperature
t	Time
β	Temperature exponent
ρ	Density
η	Combustion efficiency

Subscripts

f	Fuel
ox	Oxidizer

Acronyms/Abbreviations

CEA	Chemical Equilibrium with Applications
CFD	Computational Fluid Dynamic
FJ	Free-Jet
HDPE	High Density PolyEthylene
IR	Infrared
ISTEC	Institute of Science and Technology for Ceramics
TC	Thermo-camera
TI	Throat Insert
UHTC	Ultra-High-Temperature Ceramic
UHTCMC	Ultra-High-Temperature Ceramic Matrix Composite
UNINA	University of Naples "Federico II"

1. Introduction

The inner surface of high performance rocket nozzles, where the propellant flow is accelerated to supersonic conditions, is typically subjected to very high shear stresses and heat fluxes and high pressure in a chemically aggressive environment [1]. These severe conditions usually lead to removal of surface material due to heterogeneous reactions between oxidizing species in the hot gas and the solid wall [2]. Thus, the requirement that dimensional stability of the nozzle throat should be maintained guaranteeing a stable

engine operation makes the selection of rocket nozzle materials extremely hard.

The materials used for these applications include refractory metals, refractory metal carbides, graphite, ceramics and fiber-reinforced plastics [3, 4]. Certain classes of materials demonstrated superior performances under specific operating conditions but the choice depends on the specific application. For instance, fully densified refractory-metal nozzles generally are more resistant to erosion and thermal-stress cracking than the other materials. Graphite performs well with the least oxidizing propellant but is generally eroded severely [5, 6, 7].

In recent years, Ultra-High-Temperature Ceramic (UHTC) materials, including zirconium or hafnium diborides or carbides, are assuming an increasing importance because of their high melting points, temperature strength and oxidation resistance. Some of these materials proved to be very interesting to develop aerospace components working in harsh environments [8, 9, 10]. Bulk UHTCs with addition of silicon based ceramics, in the form of particles, short fibers or whiskers have been developed with good oxidation and ablation resistance at ultra-high temperature [11, 12]. However, due to their low fracture toughness and poor thermal shock resistance, the reliability of these materials must be improved to develop larger components with enhanced mechanical properties. Composites with continuous carbon fiber as reinforcement and UHTC or C/SiC–UHTC as matrix can be expected to perform good erosion resistance properties compared to C/C and C/SiC composites, as well as good thermal shock resistance and damage tolerance [13, 14, 15] and then to be the potential candidates for use in propulsion applications.

This so-called Ultra High Temperature Ceramic Matrix Composites (UHTCMC), are the subject of the Horizon 2020 European C^{3}HARME research project, focused on materials design and preparation, development of components from small to larger scale and testing in representative environments, including rocket nozzles [16].

In this work the results of the experimental tests carried out with a novel, dedicated test set-up exposing UHTCMC samples to the supersonic exhaust jet of a 200N-class hybrid rocket operated with gaseous oxygen burning cylindrical port High-Density PolyEthylene (HDPE) fuel grains are presented and discussed. Non-intrusive diagnostic equipment, including two-color pyrometers and an infrared thermo-camera, has been employed to monitor the surface temperature of the samples that reached values over 2800 K. The combination of combustion temperature over 3000 K, supersonic Mach number and stagnation pressures allowed reproducing realistic rocket nozzles operating conditions, in order to demonstrate the ability of the specimens to preserve their functional integrity in a relevant environment. After that a UHTCMC nozzle throat insert has been manufactured and experimentally tested to verify the erosion resistance and evaluate the effects on the rocket performance by comparison with those obtained in similar operating conditions employing a graphite nozzle.

The experimental activities are supported by proper numerical models able to predict the complex flow field in the hybrid rocket combustion chamber and the thermo-fluid dynamic conditions on the material.

2. Experimental test setup

The test rig is a versatile set up primarily designed for testing hybrid rocket engines of several sizes [17]. It is equipped with a test bench and a general-purpose acquisition system, which allow evaluating propellant performance and combustion stability [18], testing of sub-components and/or complete power systems, nozzles [19], air intakes, catalytic devices [20], burners, ignition and cooling systems [2, 21]. For the current research activities, novel, dedicated test set-up were developed to test UHTCMC materials (machine from pellets), exposing small samples to the supersonic exhaust jet of a 200N-class hybrid rocket nozzle, or a nozzle throat insert to be tested during engine operation.

A detailed description of the laboratory and of the experimental facilities can be found in Ref. [17].

The schematics of the rocket employed in this work is depicted in Fig. 1, which also shows the UHTCMC sample (in blue) behind the rocket nozzle and the nozzle insert (in red). The tests presented in the following sections were performed with a converging nozzle injector, whose exit-section diameter is 6 mm, which delivered oxygen in single-port cylindrical fuel grains of HDPE. Oxidizer mass flow rate is controlled by means of a Tescom ER3000 pressure regulator, which controls an electropneumatic valve in order to reduce the pressure to the desired setpoint, upstream a chocked Venturi nozzle. The average fuel mass flow rate is estimated by means of grain mass measurements before and after the test (see Ref. [22]).

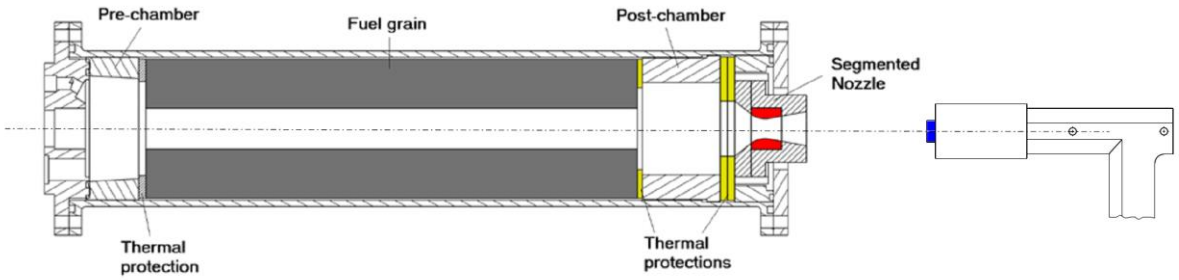

Fig. 1. Layout of 200 N-class hybrid rocket engine, including the nozzle throat insert (red) and the set-up for UHTCMC free-jet testing (blue).

As mentioned before, in the framework of the current research activities, the facility has been upgraded to allow performing tests on small, button-like samples, with maximum diameter of 17mm (Fig. 2) as a first step for the new materials characterization [23].

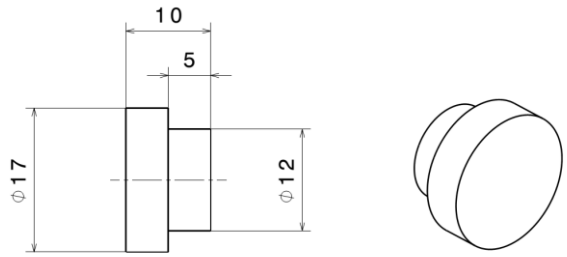

Fig. 2. Nominal design of UHTCMC samples for free-jet tests. Dimensions are in mm.

The specimen is placed downstream the hybrid rocket engine, in order to be reached by the exhaust plume coming from the nozzle. The experimental set-up consists in a mechanical system connected to the test bench in order to support and keep the specimen aligned with the motor axis. This system is designed to place the test article at the desired distance to the nozzle exit. In the present test campaign, a distance of 15 cm was selected.

Fig. 3 shows the experimental set-up, including the non-intrusive diagnostic equipment employed for the real-time evaluation of the sample surface temperature. In particular, the surface temperature of the samples can be continuously measured (±1% instrumental accuracy) by digital two-color pyrometers (Infratherm ISQ5 and IGAR6, Impac Electronic GmbH, Germany) at an acquisition rate of 100 Hz. In addition, an infrared (IR) thermo-camera (TC, Pyroview 512N, DIAS Infrared GmbH, Germany) allows for the evaluation of the temperature distribution over the sample surface. The ISQ5 pyrometer exploits two overlapping infrared wavelength bands at 0.7–1.15 μm and 0.97–1.15 μm to measure the actual temperature from 1273 K up to 3273 K. The IGAR6 pyrometer operates in the bands 1.5-1.6 μm and 2.0-2.5 μm to return the sample temperature in the range 523-2273 K. The measurement area of the ISQ5 pyrometer is approximately a round spot 3.3 mm in diameter. The thermo-camera is able to detect temperature in the range 873-3273 K and it operates in the spectral range from 0.8 to 1.1 μm. The procedure employed to set the correct value of spectral emittance, on which the IR-TC measurement is dependent, is reported in [24].

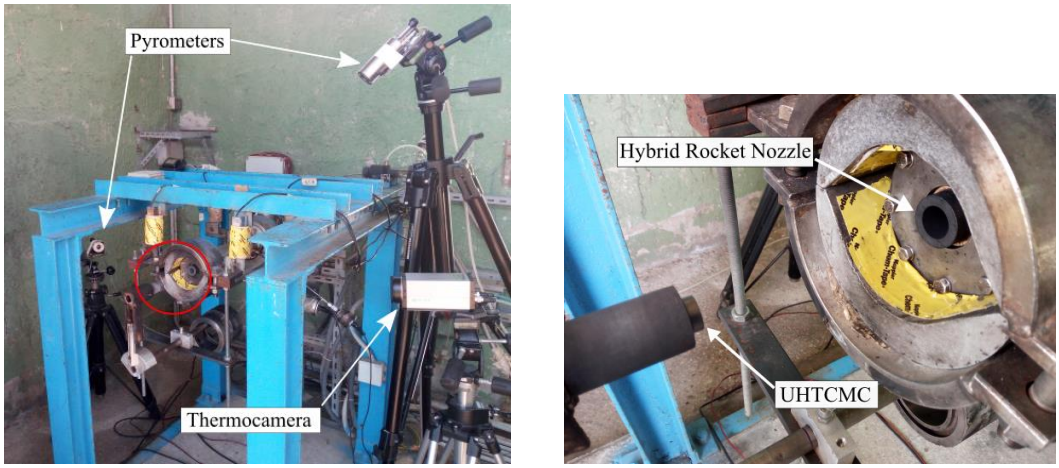

Fig. 3. Set-up for free-jet test. The area within the red circle in the left picture is zoomed in the right picture.

In the second step of the experimental characterization of the UHTCMCs, the graphite nozzle usually employed in the firing test is replaced by a segmented-designed nozzle having the outer parts, namely the converging and diverging conical elements, made of graphite, while the restricted region around the throat is made of the new materials to be tested (Fig. 4). This configuration allows to manufacture relatively small prototypes, gradually increasing the geometric complexity, and to test them to most severe conditions in terms of shear stresses and heat fluxes, which are encountered right in the nozzle throat region.

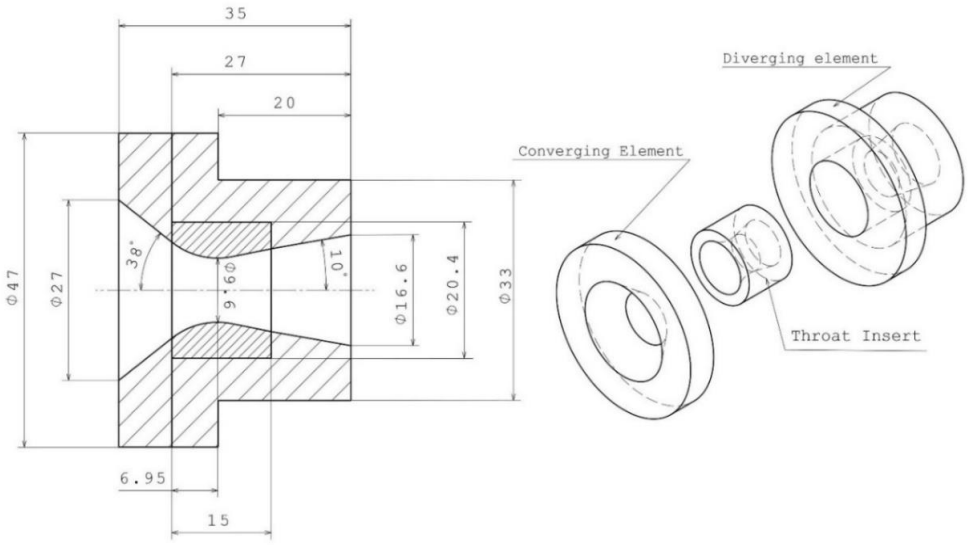

Fig. 4. Design of segmented nozzle with UHTCMC nozzle throat insert. Dimensions are in mm.

Samples and nozzle insert external surfaces were observed before and after the test by a Digital Microscope KH-8700 (HIROX-USA, Inc., United States), employing a MX(G) 5040SZ optical lens with 50-400x magnification factor. These were also measured by a digital caliper (0.01 mm accuracy).

3. Numerical models

In order to support the experimental activities, proper numerical models for the simulation of the thermo-fluid dynamic flow field inside the combustion chamber and through the nozzle of hybrid rocket engines and for the evaluation of the operating conditions around the test article have been developed, which have predictive capabilities and are able to provide additional information that are difficult to collect experimentally.

3.1. One-dimensional model for transient chamber pressure estimation

A one-dimensional model based on NASA CEA software can be used to rapidly evaluate the evolution of the operating conditions in the combustion chamber, in particular the chamber pressure, and through the nozzle during the time. In this case, the input of the model are the oxidizer mass flow rate, the geometrical dimensions of the fuel grain and the operating time.

As the instantaneous regression rate is an unknown parameter and the oxidizer mass flux and chamber pressure depend on the regression rate itself, the expected data are estimated assuming the classical regression rate law

$$\dot{r} = a G_{ox}^{n} \qquad (1)$$

where the coefficient *a* and *n* have been selected from the values available in literature relevant to the combustion of gaseous oxygen with HDPE fuel grains [25]. Integrating Eq. (1) in time, the instantaneous port diameter *D(t)* can be calculated. Then, considering the prescribed oxidizer mass flow rate, the corresponding mass flux $G_{ox}(t)$ and regression rate $\dot{r}(t)$ can be estimated. Then the fuel mass flow rate can be easily calculated as

$$\dot{m}_f(t) = \rho_f \pi D(t) L \dot{r}(t) \qquad (2)$$

where ρ_f is the solid fuel density and L is the length of the grain, and correspondingly the average mixture ratio $OF(t) = \frac{\dot{m}_{ox}}{\dot{m}_{f(t)}}$ can be derived. From these calculations, the estimation of the aft-chamber pressure p_c can be performed by means of an iterative procedure to solve the steady-state mass balance equation

$$\frac{\dot{m}_{ox}}{A_t}\left(1+\frac{1}{OF}\right)=\frac{p_c}{\eta C^*} \qquad (3)$$

in which A_t is the nozzle throat area, C^* is the theoretical characteristic exhaust velocity (that primarily depends on the mixture ratio and, to a minor degree, on pressure) and the combustion efficiency, η, has been assumed equal to unity. For the dependence of the C^* on pressure, Eq. (3) is implicit and an iterative calculation technique is needed. A combustion pressure is first assumed, then the CEA chemical equilibrium code [26] developed by NASA is run to calculate the equilibrium composition and the theoretical exhaust velocity, assuming frozen flow through the nozzle, at the given *OF* ratio in input. Finally, combustion pressure is adjusted repeatedly until convergence.

3.2. CFD model for the simulation of the flow field around test articles

In order to provide an improved understanding of test conditions around the material samples and prototypes, Computational Fluid Dynamic (CFD) simulation of the flow through the rocket nozzle and of the external plume of the exhaust gases are performed, employing as boundary conditions the time-averaged results of the numerical tool described in the previous section.

To this purpose the Reynolds-Averaged Navier-Stokes (RANS) equations for single-phase multicomponent turbulent reacting flows are solved with a control-volume-based technique and a density-based algorithm, employing the Shear Stress Transport (SST) k–ω model as turbulence closure. A detailed analysis of thermo-chemical evolution of gas mixture is performed, in order to have an accurate prediction of heat transfer at solid walls. The transport equations for the main combustion products (O_2, C_2H_4, H_2O, CO_2, CO, H_2, H, O, OH are the species considered in the current model, together with the non-reacting N_2) are solved, and the Eddy Dissipation Concept (EDC) model is employed for the combustion mechanism, which accounts for detailed chemical reaction rates in turbulent flows. Consequently, the Arrhenius rate K for each reaction is calculated as

$$K = A_K T^{\beta} \exp\left(-\frac{E_a}{RT}\right) \qquad (4)$$

where the constants have been taken from Ref. [27] and are reported in Table 1.

The Discrete Ordinates model for the radiation is included in the numerical modelling.

Table 1. C_2H_4 – O_2 reaction system.

No.	Reaction[a]	A_K[b]	β	E_a[b]
1	$C_2H_4 + O_2 \rightleftarrows 2CO + 2H_2$	1.80e+14	0.0	35500
2	$CO + O \rightleftarrows CO_2 + M$	5.30e+13	0.0	-4540
3	$CO + OH \rightleftarrows CO_2 + M$	4.40e+06	1.5	-740
4	$H_2 + O_2 \rightleftarrows OH + OH$	1.70e+13	0.0	48000
5	$H + O_2 \rightleftarrows OH + O$	2.60e+14	0.0	16800
6	$OH + H_2 \rightleftarrows H_2O + H$	2.20e+13	0.0	5150
7	$O + H_2 \rightleftarrows OH + H$	1.80e+10	1.0	8900
8	$OH + OH \rightleftarrows H_2O + O$	6.30e+13	0.0	1090
9	$H + H \rightleftarrows H_2 + M$	6.40e+17	-1.0	0
10	$H + OH \rightleftarrows H_2O + M$	2.2e+22	-2.0	0

[a]Third-body efficiencies for all thermolecular reactions are 2.5 for $M = H_2$, 16.0 for $M = H_2O$, and 1.0 for all other *M*.

[b]Units are in seconds, moles, cubic centimeters, calories and Kelvin.

The computational grid used for the simulation of the free reacting jet exiting from the nozzle is shown in Fig. 5. A pressure inlet boundary condition is set on the surface representative of the nozzle exit section, imposing the total pressure and the total temperature corresponding to the operating chamber pressure and temperature in the rocket and the static pressure and the chemical composition at the exit of the nozzle. The ambient pressure is set on the other external boundaries of the computational domain.

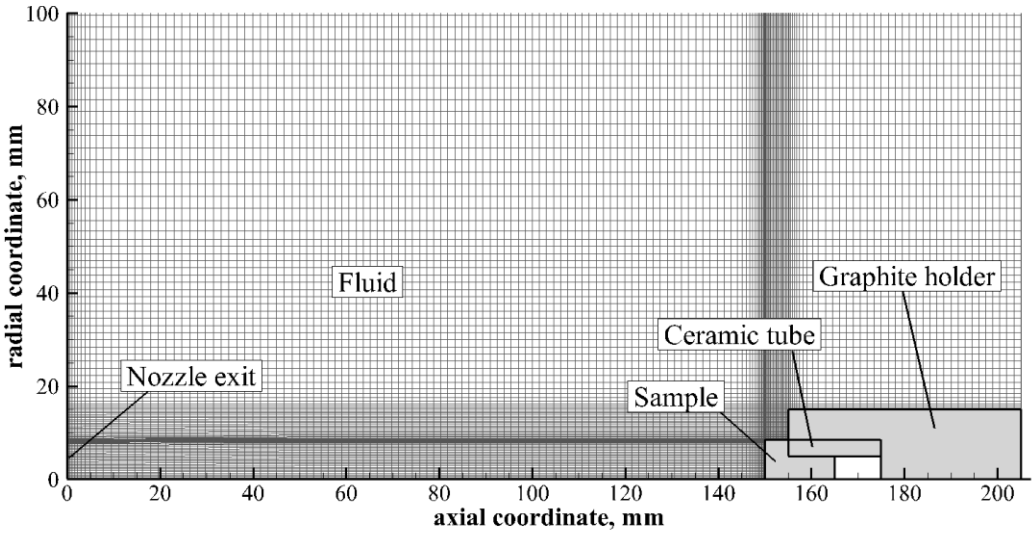

Fig. 5. Computational grid for the simulation of the free reacting jet exiting from the rocket nozzle

The typical computational grid for the simulation of the flowfield through the exhaust nozzle of the hybrid rocket is shown in Fig. 6. Similarly to what described above, a pressure inlet boundary condition is set on the inlet section of the nozzle imposing the time-averaged values of the total pressure, the total temperature and the chemical composition estimated by means of the model described in the previous section. A supersonic outlet condition is set at the exit section.

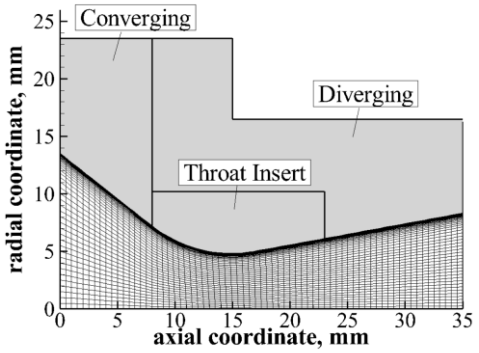

Fig. 6. Computational grid for the simulation of the flow through the rocket nozzle

4. Test conditions

Different test conditions have been selected, to evaluate the materials performance in different aero-thermo-chemical environments. All tests had a nominal duration of 10 s. Cylindrical 220mm-long HDPE grains were employed as fuel and gaseous oxygen as oxidizer.

In particular, two different set of test conditions have been considered for the free-jet test, corresponding to an oxygen mass flow rate equal to 25 g/s and to 40 g/s, respectively. In the former case, nozzles with 9.6 mm-initial diameter throat section have been employed. In the second case a 12.5 mm-throat initial diameter nozzle has been used in order to have similar values of the chamber pressure with respect to the former case, with a higher average oxidizer-to-fuel ratio, i.e. a more oxidizing chemical environment.

On the other side, for the experimental characterization of the nozzle insert, two subsequent test have been performed, again with an oxygen mass flow rate equal first to 25 g/s and then to 40 g/s. In this case, for the estimation of the nominal test conditions the nominal value of the throat diameter, equal to 9.6 mm, has been considered.

A summary of the time-averaged test conditions estimated with the numerical tool described in Sec. 3.1 is reported in Table 2.

Additional significant information can be obtained from the CFD simulations carried out with the models described in Sec. 3.2.

Fig. 7 and Fig. 8 show the distributions of temperature and molecular oxygen mass fraction, respectively, in the flow field of the free jet test, for both Test Conditions 1 and 2FJ (for a better comparison, the contours of the same quantities are plotted in the same scale for the two conditions). In particular, comparison between Fig. 7(a) and (b) verifies that the two test conditions do not differ significantly in terms of temperature distribution, as expectable due to the similar values of combustion chamber temperatures evaluated by means of the chemical equilibrium software. On the contrary, major differences are noticeable in the distribution of O_2 mass fraction, which is significantly higher in the case of Test condition 2.

Table 2. Summary of nominal time-averaged test conditions.

	Test condition 1	Test condition 2FJ	Test condition 2NI
Oxidizer mass flow rate [g/s]	25	40	40
Oxidizer-to-Fuel ratio	5.13	6.50	6.50
Chamber pressure [bar]	6.49	5.65	9.63
Combustion temperature [K]	~ 3200	~ 3200	~ 3200
Nozzle inlet CO_2 mass fraction	0.32	0.31	0.32
Nozzle inlet H_2O mass fraction	0.16	0.14	0.14
Nozzle inlet O_2 mass fraction	0.30	0.41	0.41
Nozzle exit pressure [bar]	0.42	0.46	0.73
Nozzle exit CO_2 mass fraction	0.36	0.34	0.39
Nozzle exit H_2O mass fraction	0.17	0.14	0.16
Nozzle exit O_2 mass fraction	0.30	0.41	0.41

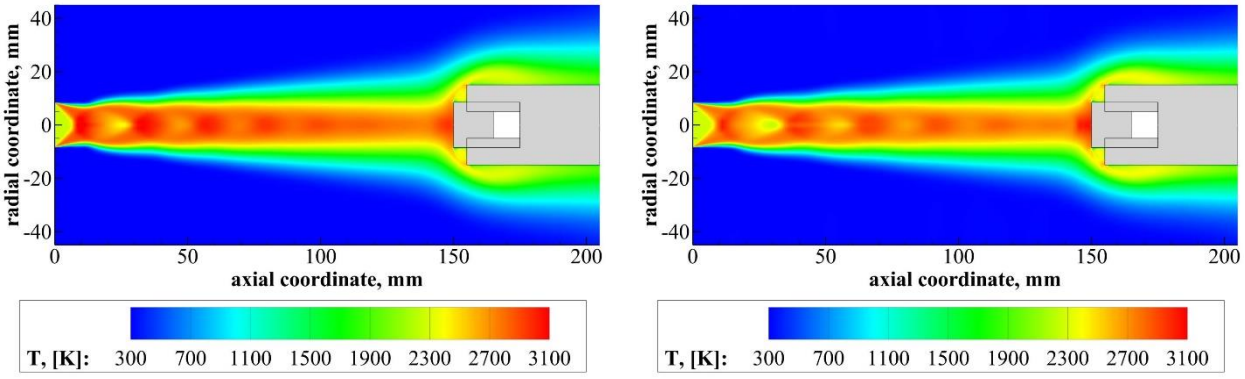

(a) (b)

Fig. 7. Temperature distribution in the free-jet test (a) for Test Condition 1 and (b) for Test Condition 2FJ.

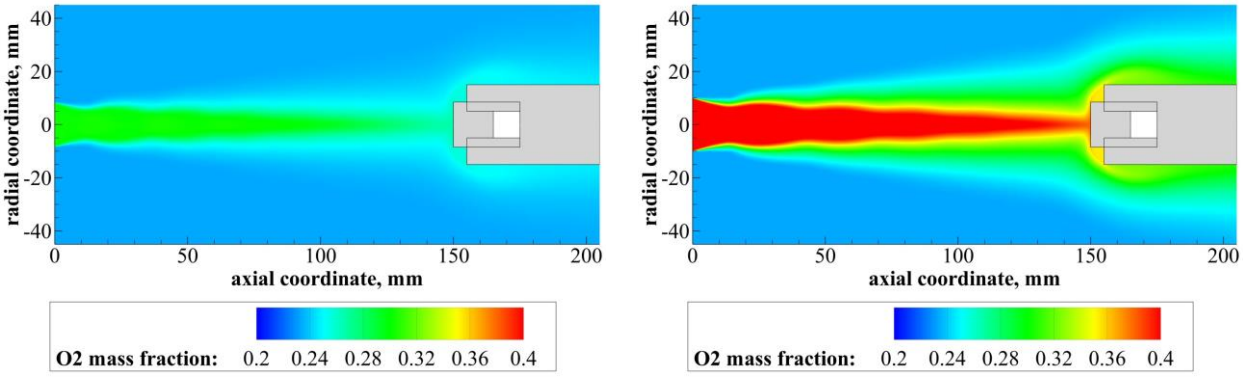

(a) (b)

Fig. 8. O_2 mass fraction distribution in the free-jet test (a) for Test Condition 1 and (b) for Test Condition 2FJ.

Similar considerations can be done for the thermo-fluid dynamic flow field through the rocket nozzle in Test conditions 1 and 2TI, as it can be observed from Fig. 9 and Fig. 10 which show the temperature and O_2 mass fraction distributions through the nozzle for the two test conditions.

Finally, Table 3 and Table 4 summarize the other significant quantities which characterize the test conditions at the sample location as estimated by the CFD simulations shown above.

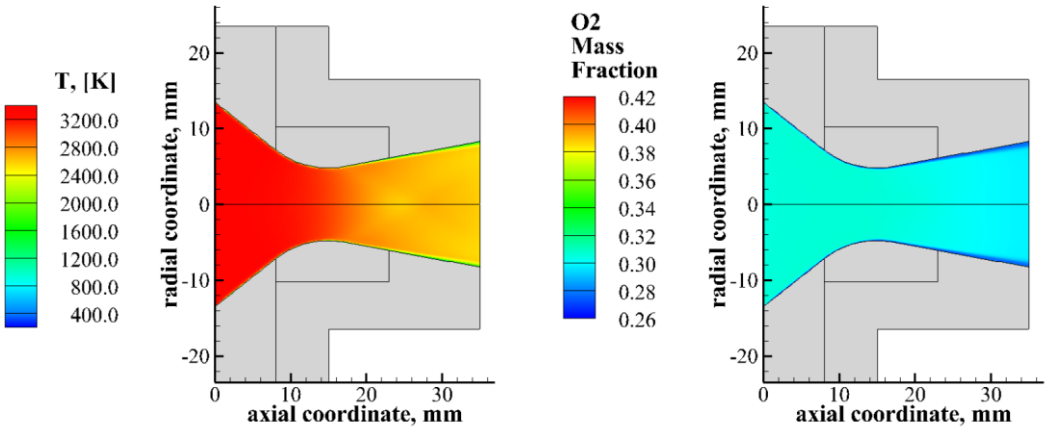

(a) (b)

Fig. 9. Temperature distribution through the rocket nozzle (a) for Test Condition 1 and (b) for Test Condition 2TI.

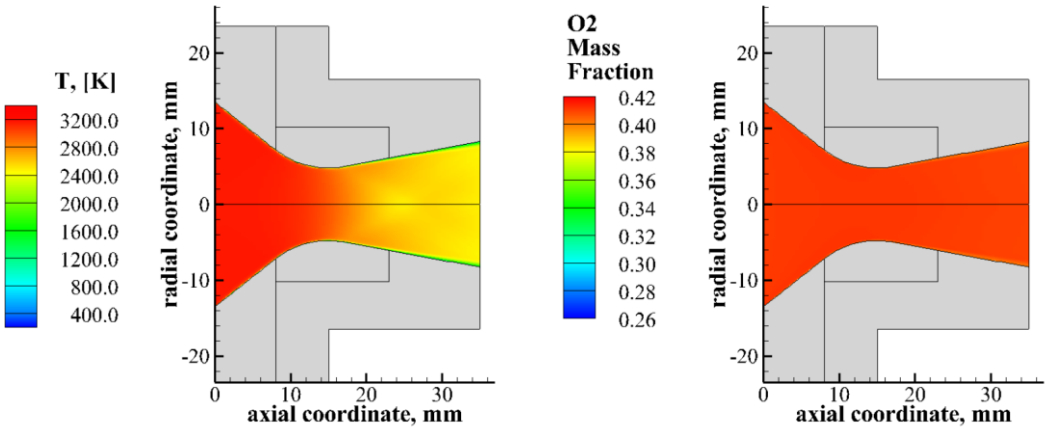

a) b)

Fig. 10. O_2 mass fraction distribution through the nozzle (a) for Test Condition 1 and (b) for Test Condition 2TI.

Table 3. Conditions at sample location estimated with the CFD simulations of the free-jet test.

	Test condition 1	Test condition 2FJ
Stagnation point pressure [bar]	2.6	3.2
Average CO_2 mass fraction	0.27	0.29
Average H_2O mass fraction	0.11	0.12
Average O_2 mass fraction	0.26	0.37
Average cold-wall surface heat flux [MW/m^2]	11.0	12.4

Table 4. Conditions at nozzle throat estimated with the CFD simulations.

	Test condition 1	Test condition 2TI
Pressure [bar]	3.2	4.8
Shear stress [hPa]	30.5	42.3
CO_2 mass fraction	0.51	0.42
H_2O mass fraction	0.22	0.18
O_2 mass fraction	0.27	0.40
Maximum cold-wall surface heat flux [MW/m^2]	17.0	20.0

5. Experimental results

5.1. Free-jet test

In a previous work [23], the authors discussed the results of some tests carried out in the free-jet configuration on samples with different compositions. These tests highlighted optimal performances of ZrB_2-SiC materials with long carbon fibers, when compared with other formulations. For this reason, in the present paper, results on this composition are presented, preliminary to the execution of tests on a nozzle-throat insert made of similar materials.

In particular, two UHTCMC samples were manufactured, based on UHTC matrix with ZrB_2 as major component and SiC as a minority phase, and continuous carbon fibers, with a 0°/90° plies architecture. They will be referred herein as UHTCMC-FJ-1 and UHTCMC-FJ-2, and were tested respectively in Test condition 1 and 2FJ.

Sample UHTCMC-FJ-1 showed an excellent resistance to the less demanding Test conditions to which it was subjected, preserving structural integrity and demonstrating an almost null erosion rate ($5 \cdot 10^{-4}$ mm/s). On the other hand, sample UHTCMC-FJ-2 was consistently eroded by the harsher aero-thermo-chemical loads, showing an erosion rate of 0.184 mm/s.

Fig. 11 and Fig. 12 show pictures of the two samples before (top) and after (bottom) test, taken by a CCD camera and the optical microscrope described in Sec. 2. In the pictures taken before the test, the continuous fiber structure of the samples is observable. The microscopic observation of the surfaces revealed the presence of a thin, irregular white layer, after the test, presumably associated to oxidation of zirconium contained in the sample matrix. The oxidized region is relatively small on UHTCMC-FJ-1, whereas almost all the exposed surface of UHTCMC-FJ-2 appears to be covered by zirconia. The more evident oxidation, associated, as said, to a considerably higher erosion rate, is explainable taking into account the higher content of oxidizing species in the flow, as exemplified by the molecular oxygen distribution presented in Fig. 10.

Fig. 13 shows the thermal histories of the two samples, detected by the pyrometer ISQ5. Sample UHTCMC-FJ-1 reached a stable and relatively low value of surface temperature, whereas sample UHTCMC-FJ-2 experienced a sudden rise in maximum temperature, which exceeded 2800 K. Finally, Fig. 14 shows two thermographic images taken during test on sample UHTCMC-FJ-2, which highlight the progressive erosion of the sample and the extremely high temperature distribution on the front surface.

The formation of a wide area of a porous and poorly-conductive oxidized phase [28, 29] could explain the observed temperature jump, and the combination of high thermal stress and oxide mechanical fragility might have triggered the significant erosion. Future micro-structural analyses will help providing a detailed interpretation of the observed phenomena.

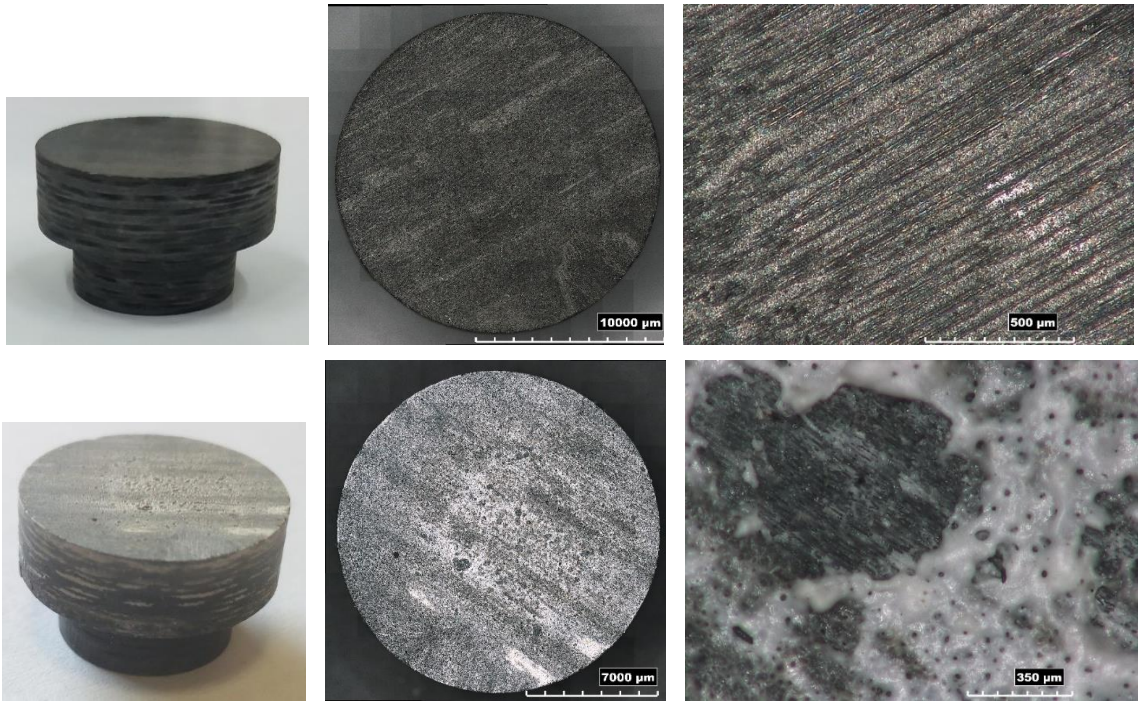

Fig. 11. Pictures of sample UHTCMC-FJ-1 before (top) and after (bottom) the test.

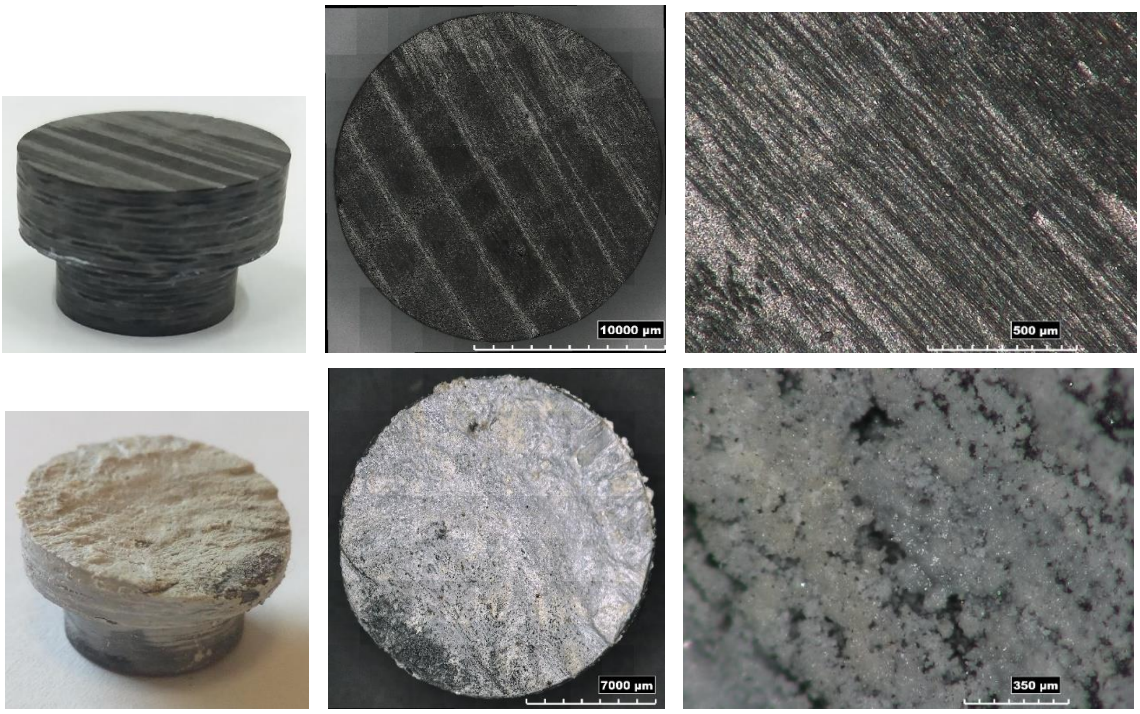

Fig. 12. Pictures of sample UHTCMC-FJ-2 before (top) and after (bottom) the test

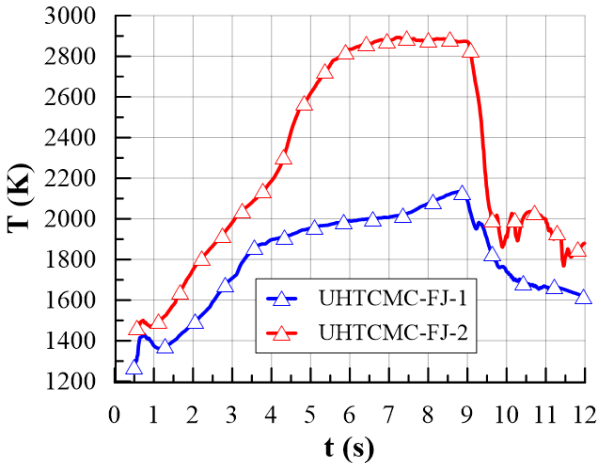

Fig. 13. Thermal histories of the two samples tested in the free-jet configuration.

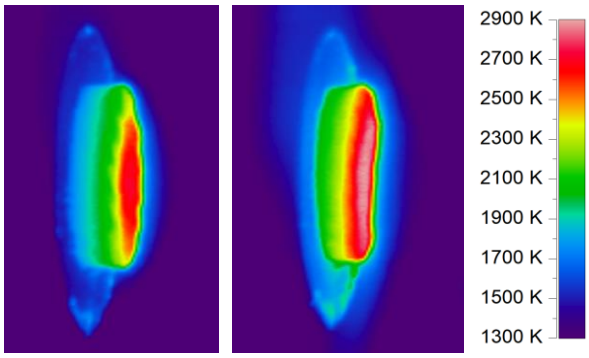

(a) (b)

Fig. 14. Thermographic images of sample UHTCMC-FJ-2 (a) at t = 5.2 s and (b) at t = 6.8 s.

5.2. Test on nozzle insert

One nozzle throat insert (which will be referred to as UHTCMC-TI), which was based, as the free-jet test samples, on a ZrB_2-SiC matrix with continuous carbon fibers, has been manufactured and tested subsequently in Test condition 1 and 2TI, to experimentally characterize its erosion resistance for rocket nozzle application. The material behavior has been compared to that of a reference graphite nozzle tested in the same test conditions.

After the first test in condition 1, it was detected that the throat diameter of the graphite nozzle increased from the nominal value of 9.6 mm to 9.9 mm, while no significant erosion occurred in the case with the UHTCMC-TI. After firing test in conditions 2TI, further considerable erosion occurred in the case of graphite nozzle, whose throat diameter increased up to around

11.4 mm. In the most severe conditions, also the UHTCMC-TI has been subjected to a perceptible erosion, which however was smaller than the former case, with an increase of the throat diameter up to 10.4 mm. The diagram in Fig. 15 graphically represents the corresponding average erosion rates, from which the improved resistance of the UHTCMC material appears clear. Fig. 16 and Fig. 17 show the pictures of the zone around the throat section before tests and after both firing tests for the graphite nozzle and the UHTCMC-TI, respectively, from which the different growth of the throat section area can be observed. Furthermore, in the latter case also an increase of the surface roughness can be noticed, probably due to the erosion of the carbon fibers which are less resistant than the ceramic matrix.

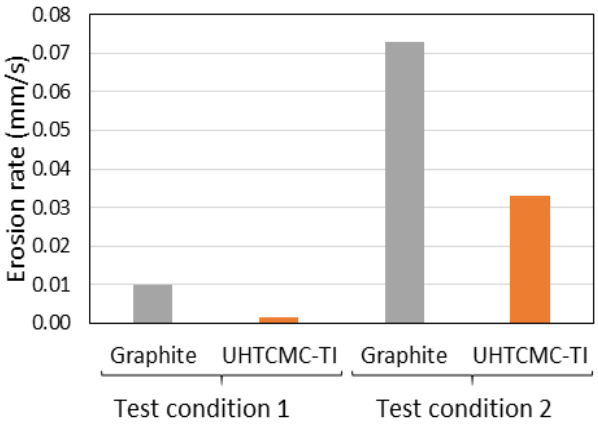

Fig. 15. Nozzle throat erosion rates.

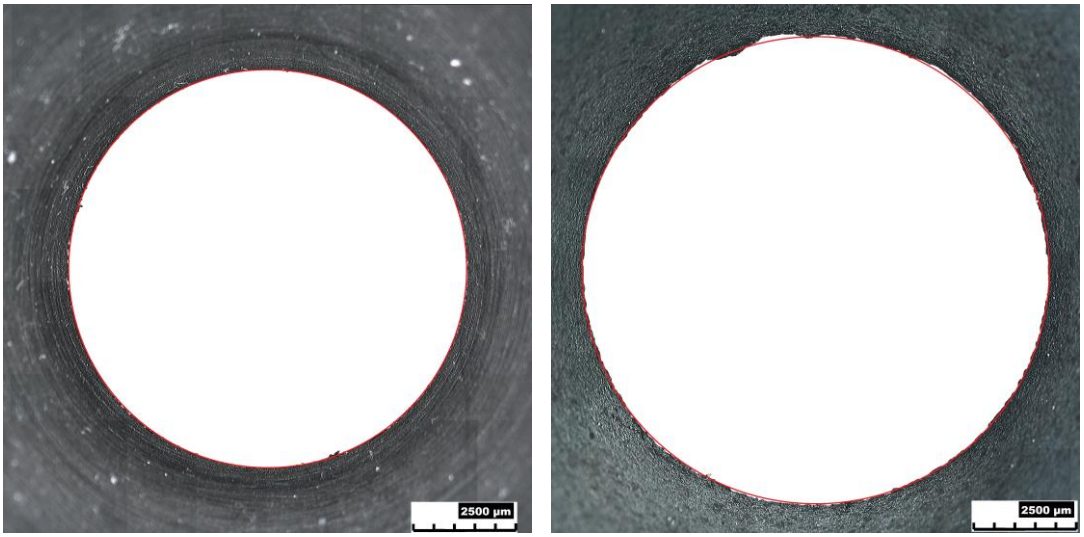

a) b)

Fig. 16. Pictures of graphite nozzle throat (a) before the tests, (b) after Test 2

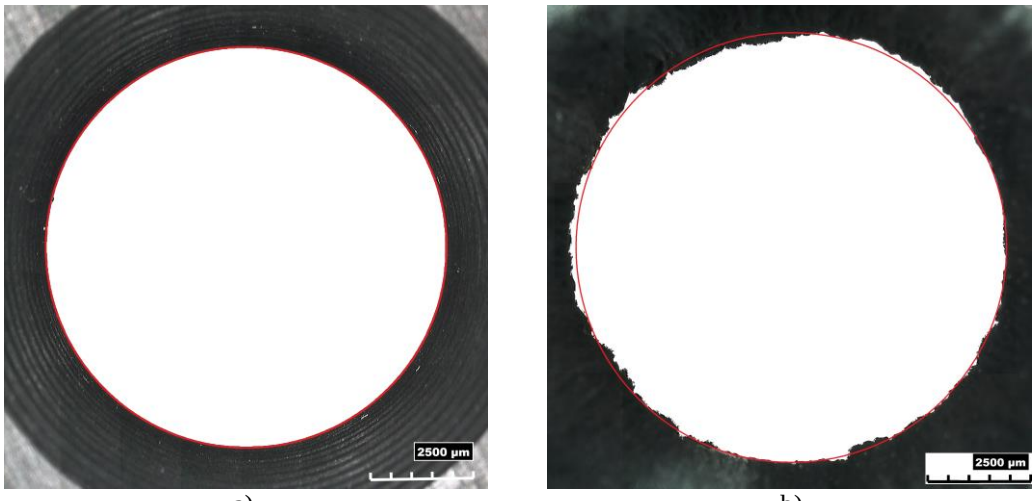

a) b)

Fig. 17. Pictures of UHTCMC-TI (a) before the tests, (b) after Test 2

The different erosion behavior highlighted above affects directly the rocket performance. Fig. 18 shows the profiles of the measured chamber pressure during the operating time and the comparison with the corresponding theoretical pressure profile estimated with the tool described in Sec. 3.1 for the two firings performed in Test conditions 2TI, in which the different behavior is more evident. In fact, in the test performed with the graphite nozzle the pressure trace shows a significantly decreasing trend due to the strong throat erosion. On the other side in the test performed with the UHTCMC-TI, the pressure trace is only slightly decreasing with respect the numerically calculated one (besides the difference due to the combustion efficiency).

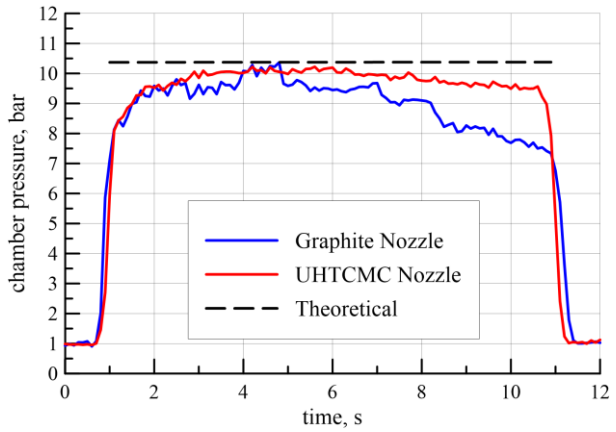

Fig. 18. Theoretical and measured chamber pressures vs operating time for tests in conditions 2TI.

6. Conclusions

An experimental campaign was carried out to characterize a new class of Ultra-High-Temperature Ceramic Matrix Composites based on ZrB_2-SiC matrix and carbon fibers, in relevant environment for nozzle rocket application. In particular, small sized samples were exposed to the supersonic flow of the exhaust gases coming from the nozzle of a 200N-class hybrid rocket at two different test conditions. The sample shows a good resistance and a stable behavior at the less severe conditions (corresponding to an oxygen mass flow rate equal to 25 g/s), while a consistent erosion was detected on the sample tested at the most severe conditions (corresponding to an oxygen mass flow rate equal to 40 g/s). The surface temperature was monitored by non-intrusive infrared equipment, including two-color pyrometers and a thermo-camera, which allowed to detect a spontaneous temperature jump of several hundred degrees in the latter case, during which maximum temperatures over 2800 K were reached. Anyway, the material shows good potentialities for application as rocket nozzle compared to other materials, as shown in a previous authors' work. Consequently, a nozzle insert made of UHTCMC (based on ZrB_2-SiC matrix and continuous carbon fibers), was manufactured and tested. The material behavior and the corresponding rocket performance were then analyzed and compared with those of a classical graphite nozzle, showing that the UHTCMC provides a better and more stable engine operation thanks to its improved erosion resistance.

Acknowledgements

The C^{3}HARME research project has received funding by the European Union's Horizon2020 research and innovation programme under the Grant Agreement n° 685594.

The authors wish to thank Prof. Claudio Leone and Dr. Silvio Genna (CIRTIBS Research Center) for technical support in realizing the microscopic pictures of the samples.

References

[1] G.D. Di Martino, S. Mungiguerra, C. Carmicino, R. Savino, Computational Fluid-dynamic Simulations of Hybrid Rocket Internal Flow Including Discharge Nozzle, AIAA 2017-5045, 53rd AIAA/SAE/ASEE Joint Propulsion Conference, 2017.

[2] R. Savino, G. Festa, A. Cecere, L. Pienti, D. Sciti, Experimental Set Up for Characterization of Carbide-Based Materials in Propulsion Environment, J. Eur. Ceram. Soc. 35 (6) (2015) 1715-1723.

[3] R. Hickman, T. Mc Kechnie, A. Agarwal, Net shape fabrication of high temperature materials for rocket engine components, AIAA 2001-3435, 37th Joint Propulsion Conference and Exhibit, 2001.

[4] J.R. Johnston, R.A. Signorelli, J.C. Freche, Performances of rocket nozzle material with several solid propellants, NASA technical note 3428.3, 1966.

[5] P. Thakre, V. Yang, Chemical erosion of carbon-carbon/graphite nozzles in solid-propellant rocket motors, J. Propuls. Power 24 (4) (2008) 822-833.

[6] J.P. Murugan, T. Kurian, J. Jayaprakash, T. Jayachandran, Design and Thermo-Structural Analysis of the Interface between Subscale Versions of Carbon-Carbon (C-C) Nozzle Divergent to Metallic flange hardware for a Ground Simulation Test, IAC-17.C2.4.8, 68th International Astronautical Congress, Adelaide, Australia, 2017.

[7] L. Kamps, S. Hirai, Y. Ahmimache, R. Guan, H. Nagata, Investigation of Graphite Nozzle-Throat-Erosion in a Laboratory-Scale Hybrid Rocket Using GOX and HDPE, AIAA 2017-4736, 53rd AIAA/SAE/ASEE Joint Propulsion Conference, 2017.

[8] M. Natali, J.M. Kenny, L. Torre, Science and technology of polymeric ablative materials for

thermal protection systems and propulsion devices: A review, Progr. Mater. Sci. 84 (2016) 192-275.

[9] G.J.K. Harrington, G.E. Hilmas, Thermal conductivity of ZrB_2 and HfB_2, in: W. Fahrenholtz, E. Wuchina, W. Lee, Y. Zhou (Eds.), Ultra-High Temperature Ceramics: Materials for Extreme Environment Applications, 1st ed., John Wiley & Sons, Inc., 2014, pp. 197-235.

[10] J. Koo, H. Stretz, J. Weispfenning, Z. Luo, W. Wootan, Nanocomposite rocket ablative materials: processing, microstructure, and performance, AIAA 2004-1996, 45th AIAA/ASME/ASCE/AHS/ASC Structures, Structural Dynamics & Materials Conference, 2004.

[11] D. Sciti, L. Zoli, L. Silvestroni, A. Cecere, G.D. Martino, R. Savino, Design, fabrication and high velocity oxy-fuel torch tests of a Cf-ZrB_2- fiber nozzle to evaluate its potential in rocket motors, Mater. Des. 109 (2016) 709–717.

[12] Y. Wang, Z. Chen, S. Yu, Ablation behaviour and mechanism of C/SiC Composites, J. Mater. Res. Technol. 5 (2016) 170-182.

[13] L. Zoli, D. Sciti, Efficacy of a ZrB2–SiC matrix in protecting C fibres from oxidation in novel UHTCMC materials, Mater. Des. 113 (2017) 207-213.

[14] L. Zoli, V. Medri, C. Melandri, D. Sciti, Continuous SiC fibers-ZrB2 composites, J. Eur. Ceram. Soc. 35 (16) (2015) 4371-4376.

[15] L. Zoli, A. Vinci, P. Galizia, C. Melandri, D. Sciti, On the thermal shock resistance and mechanical properties of novel unidirectional UHTCMCs for extreme environments, Sci. Rep. 8 (1) (2018) 9148.

[16] R. Savino, L. Criscuolo, G.D. Di Martino, S. Mungiguerra, Aero-thermo-chemical characterization of ultra-high-temperature ceramics for aerospace applications, J. Eur. Ceram. Soc. 38 (8) (2018) 2937-2953.

[17] C. Carmicino, F. Scaramuzzino, A. Russo Sorge, Trade-off between paraffin-based and aluminium-loaded HTPB fuels to improve performance of hybrid rocket fed with N2O, Aerosp. Sci. and Technol. 37 (2014) 81–92.

[18] C. Carmicino, Acoustics, Vortex Shedding, and Low-Frequency Dynamics Interaction in an Unstable Hybrid Rocket, J. Propuls. Power 25 (6) (2009) 1322–1335.

[19] A. Russo Sorge, C. Carmicino, A. Nocito, Design of a Lab-scale Cooled Two-dimensional Plug Nozzle for Experimental Tests, AIAA 2002-4039, 38th AIAA/ASME/SAE/ASEE Joint Propulsion Conference & Exhibit, 2002.

[20] S. Bonifacio, G. Festa, A. Russo Sorge, Novel Structured Catalysts for Hydrogen Peroxide Decomposition in Monopropellant and Hybrid Rockets, J. Propuls. Power 29 (2013) 1130–1137.

[21] L. Galfetti, F. Nasuti, D. Pastrone, A.M. Russo, An Italian Network to Improve Hybrid Rocket Performance: Strategy and Results, Acta Astronaut. (96) (2014) 246–260.

[22] C. Carmicino, A. Russo Sorge, Experimental Investigation into the Effect of Solid-Fuel Additives on Hybrid Rocket Performance, J. Propuls. Power 31 (2) (2015) 699–713.

[23] S. Mungiguerra, G.D. Di Martino, R. Savino, L. Zoli, D. Sciti, M.A Lagos, Ultra-High-Temperature Ceramic Matrix Composites in Hybrid Rocket Propulsion Environment, AIAA 2018-4694, 2018 International Energy Conversion Engineering Conference, AIAA Propulsion and Energy Forum, 2018.

[24] F. Monteverde, A. Cecere, R. Savino, Thermo-chemical surface instabilities of SiC-ZrB_2 ceramics in high enthalpy dissociated supersonic air flows, J. Eur. Ceram. Soc. 37 (6) (2017) 2325-2341.

[25] A. Karabeyoglu, G. Zilliac, B.J. Cantwell, S. De Zilwa, P. Castellucci, Scale-Up Tests of High Regression Rate Paraffin-Based Hybrid Rocket Fuels, J. Propuls. Power 20 (6) (2004) 1037-1045.

[26] S. Gordon, B.J. McBride, Computer Program of Complex Chemical Equilibrium Compositions and Applications, NASA Reference Publication 1311, 1994.

[27] D.J. Singh, C.J. Jachimowski, Quasigobal Reaction Model for Ethylene Combustion, AIAA J. 32 (1) (1994) 213-216.

[28] Z. Deng, J.M.F. Ferreira, Y. Tanaka, Y. Isoda, Microstructure and thermal conductivity of porous ZrO_2 ceramics, Acta Mater. 55 (11) (2007) 3663-3669.

[29] K.W. Schlichting, N.P. Padture, P.G. Klemens, Thermal conductivity of dense and porous yttria-stabilized zirconia, J. Mater. Sci. 36 (2001) 3003-3010.